

Article

Mineralogy and Garnet Sm–Nd Dating for the Hongshan Skarn Deposit in the Zhongdian Area, SW China

Bo Zu ¹ , Chunji Xue ^{2,*}, Chen Dong ³ and Yi Zhao ⁴¹ School of Earth Resources, China University of Geosciences, Wuhan 4330074, China; zubo@cug.edu.cn² State Key Laboratory of Geological Processes and Mineral Resources, Faculty of Earth Sciences and Resources, China University of Geosciences, Beijing 100083, China³ Jiangxi Institute of Geological Exploration for Mineral Resources of Nonferrous Metals, Nanchang 330025, China; chendcugb@163.com⁴ Yunnan Geological Survey, Kunming 650051, China; ttrainy@163.com

* Correspondence: chunji.xue@cugb.edu.cn; Tel.: +86-10-8232-1895

Received: 23 February 2019; Accepted: 17 April 2019; Published: 19 April 2019



Abstract: The Hongshan deposit is one of the largest Cu-polymetallic deposits in the Zhongdian area, southwest China. Two types of Cu–Mo ores, mainly developed in the skarns, have been recognized in the Hongshan deposit, i.e., massive or layered skarn and vein-type, with the former being dominant. The highly andraditic composition of garnet (Adr₁₀₀ to Adr₆₄Gr₃₂) and diopsidic composition of pyroxene (Di₉₀Hd₉ to Di₁Hd₉₉) indicate the layered skarn ores are of magmatic-hydrothermal origin that formed under oxidized conditions. Sm–Nd dating of garnet yield a well-constrained isochron age of 76.48 ± 7.29 Ma (MSWD = 1.2) for the layered skarn ores. This age was consistent with the Re–Os age for the pyrrhotite from the layered skarn ores, and thereby indicated that the layered skarn mineralization was formed in the Late Cretaceous, rather than in the Triassic as was previously thought. The coincidence of the geochronology from the layered skarn ores and vein-type mineralization further indicated that both ores were the result of a single genetic event, rather than multiple events. The recognition of the Late Cretaceous post-collisional porphyry–skarn Cu–Mo–W belt in the Zhongdian area exhibited a promising prospecting potential.

Keywords: skarn mineralogy; high fugacity; garnet Sm–Nd dating; Late Cretaceous; Hongshan skarn deposit

1. Introduction

The Zhongdian Cu-polymetallic area, situated in the southern segment of the Yidun arc (Figure 1a,b), is commonly regarded as one of the most fertile regions for porphyry and skarn copper deposits in China [1–3]. Many of the porphyry copper deposits in the Zhongdian area (Figure 1c), such as Pulang (803.85 Mt with 0.52% Cu, 0.18 g/t Au, [4,5]), Xuejiping (54.15 Mt with 0.53% Cu, 0.06 g/t Au), Langdu (1.67 Mt with 6% Cu), Chundu, and Lannitang (36 Mt with 0.50% Cu, 0.45 g/t Au) deposits were formed in the Late Triassic as a result of westward subduction of the Garzê–Litang oceanic crust [4,5]. Recently, the recognition of some Late Cretaceous porphyry–skarn deposits, represented by the Hongshan Cu–Mo, Tongchanggou Mo–Cu, Xiuwacu W–Mo, and Relin W–Mo deposits, has drawn much attention on the collision-related metallogeny of the Zhongdian area [6–9].

The Hongshan deposit is one of the largest Cu-polymetallic deposit in the Zhongdian area (Figure 1c) with contained metals of 0.64 t Cu, 5769 t Mo, 7532 t W, 323 t Ag, and 25262 t Pb + Zn [10]. Generally, two types of ores, namely the major layered skarn Cu-polymetallic ores and later vein-type

Cu–Mo mineralization, have been formed [9,11]. Trace elements of pyrite and pyrrhotite from both types display distinct signatures and could plausibly indicate different origins [10]. Previous research proposed a two-stage model for the genesis of the Hongshan deposit with Triassic skarn Cu–polymetallic ores overprinted by Late Cretaceous vein-type Cu–Mo mineralization [10,11]. The age of later vein-type Cu–Mo mineralization has been well-constrained by molybdenite Re–Os and zircon U–Pb ages [9,11,12]. The mineralization age of the layered skarn Cu–polymetallic ores, however, has been poorly constrained. Zu et al. reported a Cretaceous age for the layered skarn ores using Re–Os dating on pyrrhotite [9]; however, the closure temperature of Re–Os systems for pyrrhotite is as low as 400 °C and might have undergone osmium diffusion or resetting in the presence of a later stage overprint event [13,14]. Thus, the timing of the layered skarn ores is still one key problem with the two-stage model.

A number of studies have indicated that garnets are useful geochemical tracers and can be used in geochronological studies [15,16]. In this contribution, we report systematic petrography and geochemistry of the main skarn mineral and Sm–Nd isotope systematics of garnet for layered skarn ores in the Hongshan deposit. The results, combined with the previous data, allow us to constrain the mineralization age of the skarns and to explain the genesis and geologic setting of the Hongshan Deposit. The implications for Cretaceous metallogeny in the Zhongdian area are also discussed.

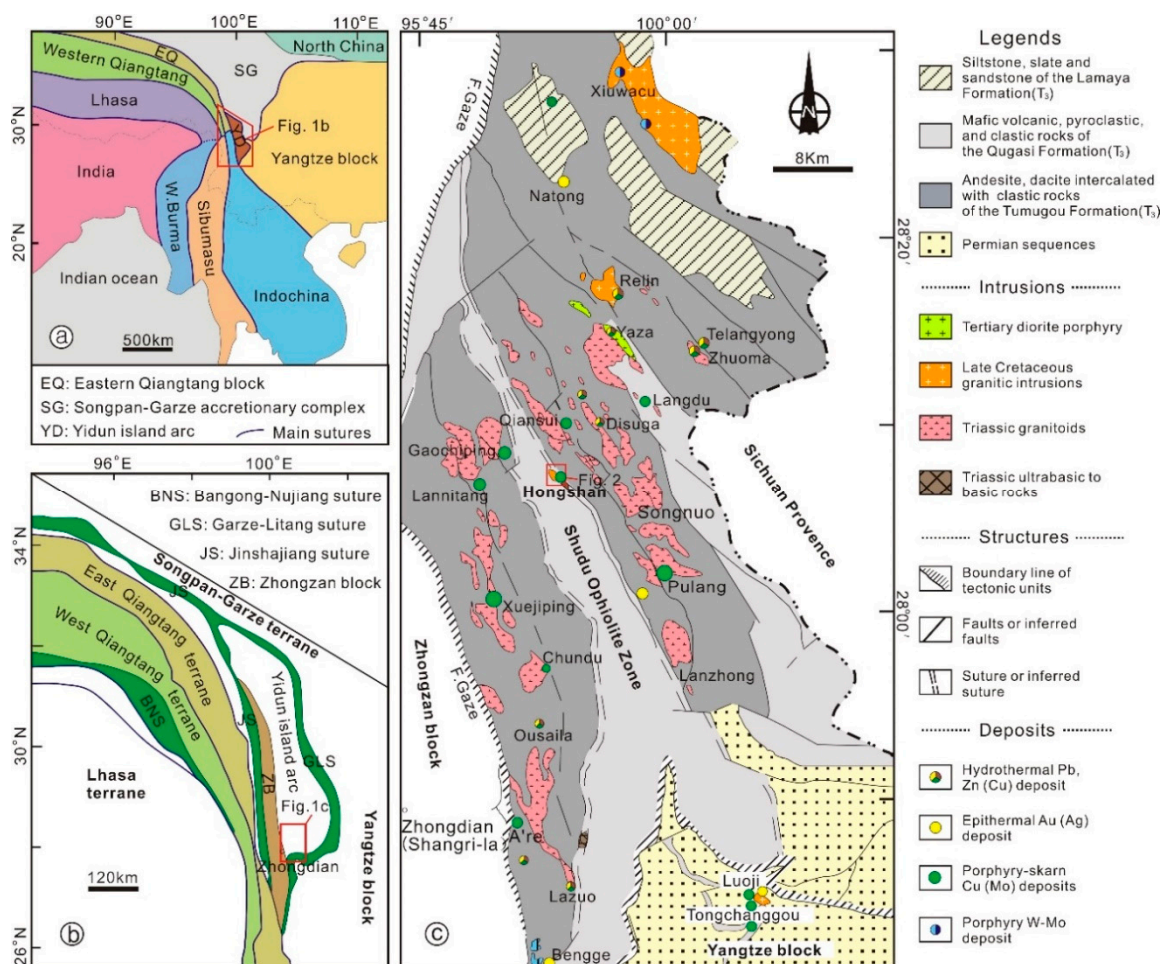


Figure 1. (a) Tectonic map sketch showing the distribution of principal continental blocks and sutures of Southeast Asia. The location and outline of the Yidun island arc are indicated. (b) Tectonic framework of the Sanjiang Tethyan domain and location of the southern Yidun arc. (c) Geological map showing the distribution of porphyry and skarn deposits in the southern Yidun arc. Modified from Zu et al. and Deng et al. [1,17].

2. Geological Setting

The Zhongdian area is located at the southern end of the Yidun island arc, forming a significant metallogeny belt in the Sanjiang Tethyan metallogenic domain (Figure 1b) [15,16]. The main tectonic framework of the Yidun arc is defined by the Garzê–Litang suture belt to the south and east and the major Dege–Xiangcheng fault to the west separates it from Zhongzan massif (Figure 1c) [9,18].

The southern Yidun arc witnessed a complex tectonic evolution history including Triassic oceanic crustal subduction, Jurassic–Cretaceous continental collision, and Cenozoic regional strike-slip faulting [18–20]. In the Triassic, westward subduction of the Garzê–Litang ocean led to the formation of the Yidun arc in the eastern part of the Zhongzan block, accompanied by the formation of voluminous volcanic and granitic rocks with ages mainly from 238 to 210 Ma (Figure 1c) [20,21]. These volcanic and granitic rocks host numerous mineral deposits, such as the Gacun volcanic massive sulfide (VMS) Ag-polymetallic deposit and porphyry–skarn deposits that were formed in a compressional setting (Figure 1c), in association with subduction of different angles [22]. When the Garzê–Litang ocean closed completely at the end of the Triassic, the Yidun island arc collided with the Yangtze block, accompanied by the emplacement of sparsely distributed granites from 138 to 75 Ma. Mineral deposits formed in this period of time, such as the Xiuwacu, Relin, Hongshan, and Tongchanggou deposits [8,23]. During the Cenozoic, a remote response to the Indian–Asian continental collision caused intracontinental strike-slip processes with the emplacement of alkaline granite intrusions and associated Au mineralization within the southern Yidun arc, including the Yaza and Bengge deposits (Figure 1c).

3. Geology of the Hongshan Deposit

The Hongshan Cu-polymetallic deposit is located in the central part of the Zhongdian area (Figure 1c). The main country rocks of the deposit comprise mainly a thick Triassic sequence of crystalline limestone, siltstone, gray to very dark gray argillaceous slate, and interlayered andesitic tuff of the Upper Triassic Qugasi formation (Figure 2). These rocks underwent contact thermal and replacement metamorphism with the development of extensive hornfels, marble and skarn throughout the deposit and surrounding areas (Figure 3).

Sparse felsic dikes and offshoots are exposed in the Hongshan deposit area. Diorite porphyries are the most widely distributed, and occur mainly in the southeastern and northern parts of the deposit area with SHRIMP U–Pb ages of 214 ± 2 Ma [17]. However, a direct contact between these porphyries and the orebodies has not been observed in the Hongshan deposit (Figure 2a). Quartz monzonite porphyry outcrops only as three small intrusions in the middle of the Hongshan area; a small part of the quartz monzonite porphyries have been altered to endoskarn near contact zones with marble (Figure 3a). Boreholes CK 17-2 and CK 17-4 have revealed concealed mineralized stocks that may be larger than the outcrops (Figure 2b,c) [17]. Previous dating suggests that the quartz monzonite porphyry and the concealed granite porphyry were formed in Late Cretaceous with zircon U–Pb ages of 77–81 Ma [12,17,23].

The copper orebodies in the study area are sheet-like, tabular, or lenticular; are subparallel to the main NNW-striking structures in the deposit area; and are hosted by skarn and hornfels zones. Individual orebodies generally strike NNW and range from 30 to 1223 m in length along strike, 20 to 420 m in width along the dip direction, and 3.9 to 19.6 m in thickness. Based on mineral assemblages and ore textures, two types of Cu–Mo ores, mainly developed in the skarns, have been recognized, i.e., massive or layered skarn (Figure 3a) and vein-type, with the former being dominant. Some other ore types are also present: hydrothermal Pb–Zn ores in the periphery of the Hongshan deposit (Figure 2a), and Mo–Cu porphyry ores associated with concealed intrusions at depth [17]. The alteration and mineralization in the Hongshan deposit can be divided into three alteration stages. The early stage (stage 1) is characterized by the alteration of wallrocks to albite–biotite–quartz–andalusite hornfels and massive, sage-green diopside hornfels (Figure 3d–f). In the skarn stage (stage 2), the interaction between the magmatic hydrothermal fluids and marble resulted in diverse assemblages

of calc–silicate skarn minerals including garnet, diopside, wollastonite, and magnetite. The early retrograde alteration stage (stage 3a) is characterized by hydrosilicate minerals and sulfide minerals overprinting on the calcsilicate minerals, forming the massive and disseminated skarn ores (Figure 3b,c). The quartz–sulfide stage (stage 3b) featured a variety of quartz–sulfide veins overprinting skarns and hornfels. Marble-hosted hydrothermal Pb–Zn mineralization scattered on the periphery of the Cu–Mo skarn orebodies (Figure 2a), exhibiting a clear mineralization zoning.

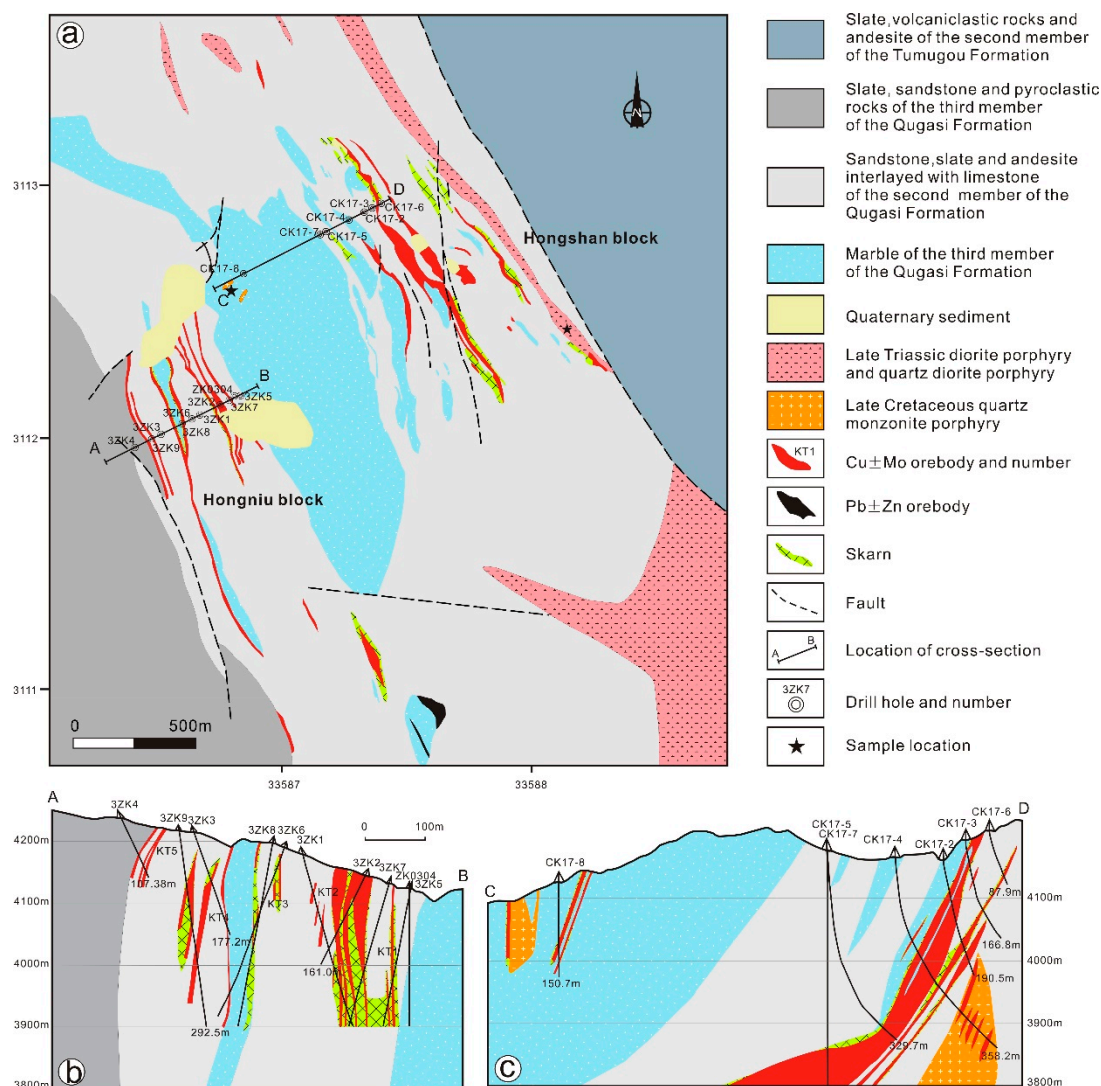


Figure 2. Simplified geological map (a) and cross-sections (b,c) of the Hongshan Cu–Mo deposit. Modified from Wang et al. [23].

The spatial zonation of the skarn minerals in the Hongshan deposits are also apparent with at least three associations. The endoskarns are only present within the quartz monzonite porphyry and have a mineral assemblage of garnet, diopside, and vesuvianite (Figure 3a) [17]. Exoskarns are more widely developed with a mineral assemblage of garnet, diopside, fluorite, and actinolite in the massive or layered skarn ores (Figure 3b,c). Minor distal skarns are scattered in the periphery of the main orebodies and associated with marble, hornfels, or wollastonite (Figure 3d–f). Garnet is the most abundant mineral in different assemblages and several different garnet generations can be optically distinguished. Garnets in the endoskarns are reddish, fine-grained, anisotropic, and have dodecahedral and/or polysynthetic twinning (Figure 3a). Garnets in the exoskarns are isotropic and euhedral, anisotropic (Figure 3j,k), and display evident oscillatory zoning (Figure 3g–i). The epitaxial

growth with oscillatory zoning exoskarn garnets indicate these garnets might have formed during different stages (Figure 3g). Garnets from the distal skarns are greenish, brown, and rarely reddish in color without apparent oscillatory zonings (Figure 3l).

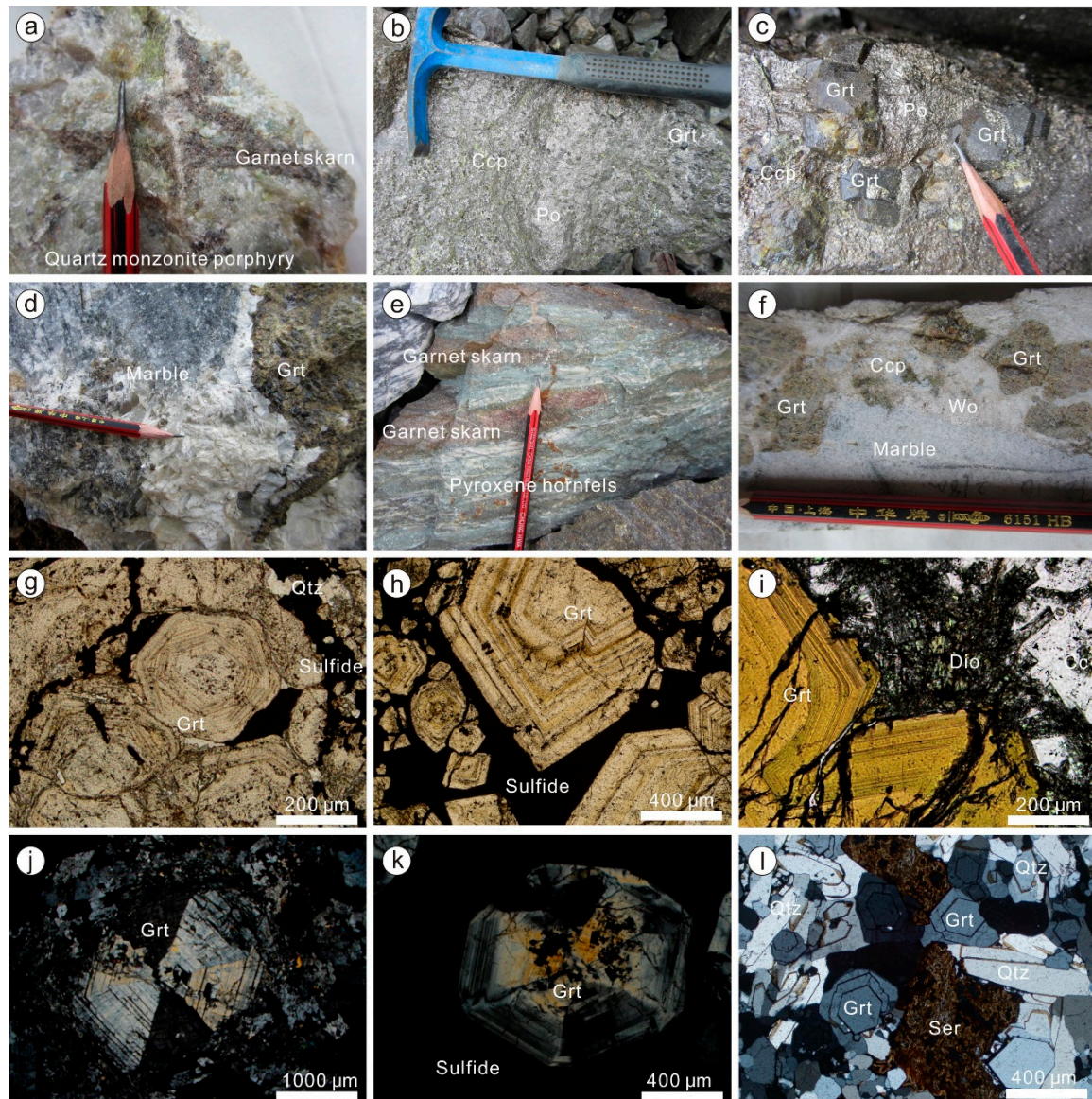


Figure 3. Photographs and photomicrographs showing characteristics of skarn ores in the Hongshan deposit. (a) Garnet in endoskarn in contact with residual quartz monzonite porphyry. (b) Massive or layered skarn ores with dense disseminated pyrrhotite in exoskarn. (c) Euhedral garnet in exoskarn ores with dense disseminated pyrrhotite and chalcopyrite. (d) Greenish-brown garnet in distal skarns along the marble. (e) Reddish-brown distal skarn in pyroxene hornfels. (f) Brown euhedral garnet along with marble and wollastonite. (g–k) Garnets in the exoskarns are isotropic and euhedral, anisotropic, and display evident oscillatory zoning. (l) Garnet from distal skarn lacks of apparent oscillatory zonings. Ccp: chalcopyrite, Dio: diopside, Grt: garnet, Po: pyrrhotite, Qtz: quartz, Ser: sericite, Wo: wollastonite

4. Sampling and Analytical Methods

Polished sections were used to study skarn minerals following by electron microprobe analyses on representative garnet, pyroxene, and tremolite (actinolite). Major element analyses of these minerals were carried out at the China University of Geosciences (Beijing) using a Shimadzu EPMA-1600. An accelerating voltage of 25 kV, a beam current of 20 nA, and a beam diameter of 1 μm were applied.

Natural minerals and synthetic oxides were used as standards, and all data were corrected using standard ZAF correction procedures.

Ten skarn-bearing samples from the layered skarn ores in the Hongshan deposit were collected to pick pure garnet separates from high precision Sm–Nd isotope systematic analyses. Pure garnet separates were handpicked under a binocular microscope to select grains similar in appearance to the chips of the 60–80 mesh size crushed by agate mortar, and then powered to <200 mesh size. Sm–Nd isotopic analyses were performed on a ISOPROBE-T thermal ionization mass spectrometry (TIMS) at the Beijing Research Institute of Uranium Geology.

5. Analytical Results

5.1. Mineral Composition

Electron microprobe analyses show that garnets from the deposit form a grossular–andradite solid solution and dominated with andradite (Tables 1–3). Forty-nine spots on garnet grains from exoskarn from this study range from almost pure andradite (Adr_{100}) to $\text{Adr}_{64}\text{Gr}_{32}$ with less than 5% of other types of garnets (Figure 4a). They contain significant less Al contents than the garnets from endoskarn ($\text{Adr}_{22-57}\text{Grs}_{78-43}$) and from distal skarn ($\text{Adr}_{14-60}\text{Grs}_{86-40}$) [24]. Oscillatory zoned garnets are generally chemically zoned with fluctuation-ore repeated changes of FeO_T content and Al_2O_3 content (Figure 5). The invariably negative correlation between FeO_T and Al_2O_3 compositions also indicate the common existence of grossular–andradite solid solution (Figure 5).

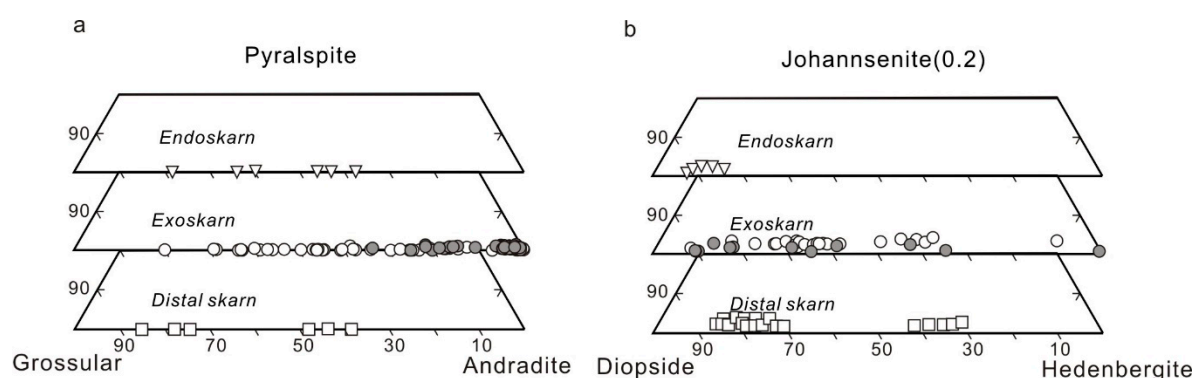


Figure 4. Major element compositions of garnets (a) and pyroxene (b) showing their dominance of end members from three selected skarn mineral deposits. Pyralspite–(pyrope + spessartine + almandine + uvarovite).

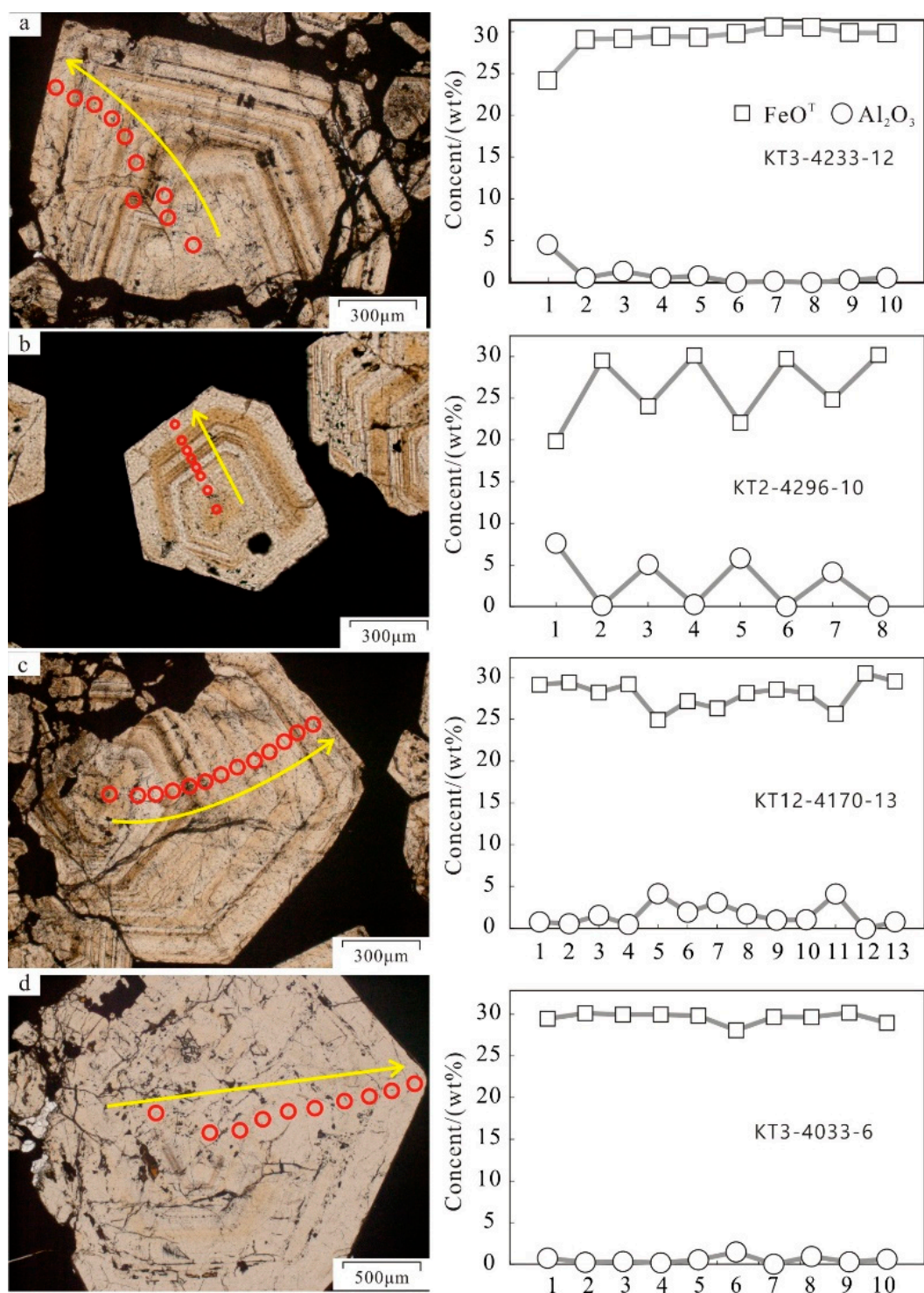


Figure 5. Variation of FeO_T and Al₂O₃ content from core to margin in the garnet grains from the layered skarn ores.

The pyroxene (12 spots) from the Hongshan deposit are mainly diopside in composition, with minor hedenbergite and rarely johannsenite (Figure 4b). The composition of the pyroxene from the exoskarn has large variations with Di90Hd9 to Di1Hd99 (Table 4).

The prograde garnet, pyroxene, and wollastonite are commonly overprinted by retrograde tremolite, actinolite, epidote, and minor chlorite. The actinolite minerals (6 spots) in this study belongs to ferro-actinolite with high amounts of MgO (19–22 wt %) and FeO_T (5–11 wt %) (Table 5).

5.2. Sm–Nd Dating Result

The Sm and Nd concentrations and isotopic ratios of garnets from the Hongshan deposit are listed in Table 6 and plotted in Figure 6. All the 10 analyzed samples showed a roughly linear correlation with an isochron age of 60.91 ± 4.94 Ma (MSWD = 26) (Figure 6a) using IsoplotR [25]. Three garnet samples (D21-5, D48-13, and KT2-4296-6) deviate the isochron line and could plausibly represent the incorporation of other minerals or/and affected by later perturbation despite detailed petrography study before analyzing (Figure 6a). The remaining 7 samples revealed a well-constrained isochron age of 76.48 ± 7.29 Ma (MSWD = 1.2) (Figure 6b), which represents the crystallization time of the garnet. The uncertainty of ± 7.29 Ma is due to low $^{147}\text{Sm}/^{144}\text{Nd}$ ratios (<0.30) rather than low precision of the Nd isotope ratios.

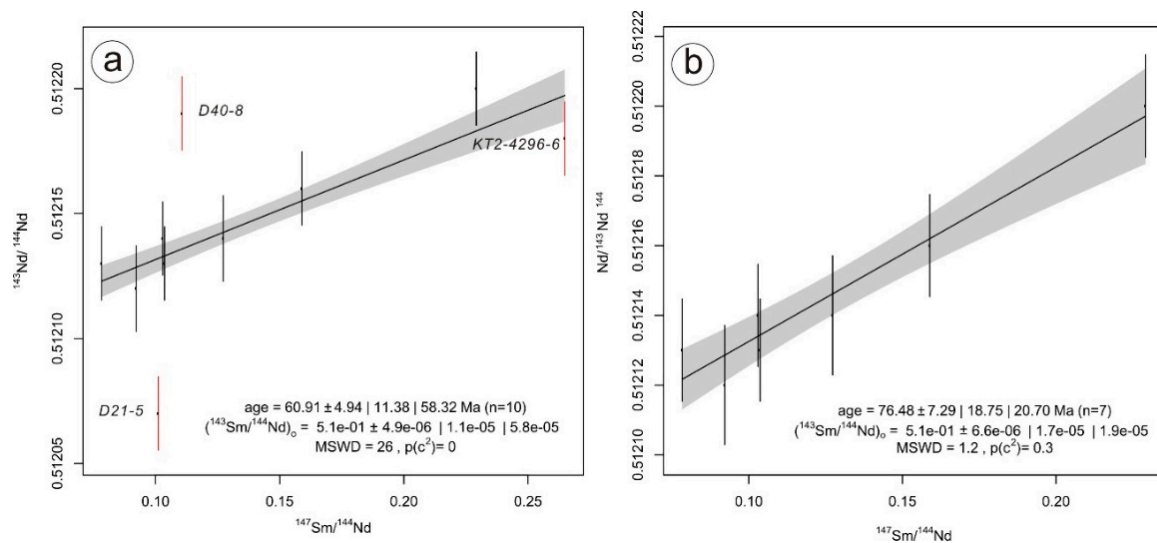


Figure 6. Sm–Nd garnet from the layered skarn ore in the Hongshan deposit. Age provided in (a) is calculated from all of the plotted data and age in (b) is calculated from seven garnet samples.

Table 1. Electron microprobe analyses of garnet from the Hongshan deposit (wt %).

Sample	Garnet–Diopside Skarn										Garnet–Diopside Skarn				
	KT3-4033-12										KT4-4078-1				
	Core			→			Rim				Core		→	Rim	
SiO ₂	36.21	35.74	35.48	35.48	35.26	35.46	35.27	35.44	35.36	35.29	36.44	36.45	36.32	35.92	35.94
TiO ₂	0.10	0	0	0	0.02	0	0	0	0.03	0.03	0.20	0.21	0.20	0.04	0.11
Al ₂ O ₃	4.54	0.57	1.36	0.56	0.79	0.02	0.16	0	0.32	0.57	5.02	3.56	5.19	3.92	4.11
Cr ₂ O ₃	0.04	0.09	0.10	0.07	0.06	0.17	0	0.05	0.25	0.09	0.17	0.12	0.12	0.16	0
FeO	24.12	29.01	29.11	29.39	29.27	29.72	30.51	30.45	29.83	29.78	22.74	23.95	23.03	24.53	24.40
MnO	0.28	0.47	0.38	0.38	0.45	0.36	0.44	0.40	0.29	0.37	0.36	0.46	0.34	0.19	0.22
MgO	0.14	0.19	0.15	0.16	0.03	0.20	0.11	0.11	0.10	0.11	0.22	0.21	0.33	0.21	0.10
CaO	33.01	32.21	32.06	32.82	32.41	32.31	32.12	32.36	32.30	32.63	33.00	33.06	33.06	33.34	33.81
Na ₂ O	0.15	0.14	0.05	0.08	0.03	0.06	0.05	0.15	0.17	0.08	0.20	0.20	0.23	0.11	0.24
K ₂ O	0	0	0	0	0	0	0	0	0	0	0	0	0	0	0
Total	98.59	98.42	98.69	98.94	98.32	98.30	98.66	98.96	98.65	98.95	98.35	98.22	98.82	98.42	98.93
Number of cations on the basis of 12 O															
Si	2.97	2.98	2.96	2.95	2.95	2.97	2.95	2.96	2.96	2.94	2.99	3.00	2.97	2.96	2.95
Ti	0.01	0	0	0	0	0	0	0	0	0	0.01	0.01	0.01	0	0.01
Al	0.44	0.06	0.13	0.05	0.08	0	0.02	0.00	0.03	0.06	0.48	0.35	0.50	0.38	0.40
Fe ³⁺	1.57	1.95	1.89	1.97	1.95	2.01	2.02	2.02	1.98	1.98	1.51	1.64	1.51	1.63	1.63
Fe ²⁺	0.08	0.08	0.14	0.07	0.10	0.08	0.12	0.10	0.11	0.10	0.05	0.01	0.07	0.06	0.04
Mn	0.02	0.03	0.03	0.03	0.03	0.03	0.03	0.03	0.02	0.03	0.02	0.03	0.02	0.01	0.02
Mg	0.02	0.02	0.02	0.02	0.00	0.02	0.01	0.01	0.01	0.01	0.03	0.03	0.04	0.03	0.01
Ca	2.90	2.88	2.86	2.93	2.91	2.90	2.88	2.90	2.90	2.91	2.90	2.92	2.89	2.94	2.97
And	78.07	96.91	93.10	97.07	95.96	99.34	99.22	99.84	97.63	96.96	75.23	82.25	74.82	80.69	80.41
Gro	17.85	1.66	0.55	1.25	0.67	4.11	4.66	4.77	3.14	1.86	20.74	15.02	20.52	15.67	17.27
Pyr	0.57	0.78	0.61	0.65	0.12	0.82	0.45	0.45	0.41	0.45	0.90	0.86	1.33	0.85	0.40

Table 2. Electron microprobe analyses of garnet from the Hongshan deposit (wt %).

Sample	Garnet–Diopside, Exoskarn											Diopside–Garnet Skarn				
	KT12-4170-13											KT2-4235-10				
	Core			→			Rim					Core		→	Rim	
SiO ₂	35.42	35.46	35.58	35.51	35.49	35.82	35.90	35.48	35.49	36.00	35.76	35.44	35.26	35.73	34.82	35.64
TiO ₂	0	0.12	0	0	0.11	0.08	0.03	0	0.09	0	0.06	0.07	0.11	0	0.02	0
Al ₂ O ₃	0.80	0.58	1.58	0.50	4.19	1.97	3.09	1.74	1.01	1.06	4.16	0	0.81	0.17	0.08	0.03
Cr ₂ O ₃	0.02	0.25	0	0	0	0	0.06	0.01	0	0.07	0.12	0	0.05	0.09	0.00	0.05
FeO	29.26	29.54	28.32	29.31	25.03	27.28	26.41	28.26	28.68	28.29	25.77	30.61	29.66	30.12	30.26	30.15
MnO	0.23	0.18	0.09	0.08	0	0.37	0.15	0.02	0.23	0.26	0.26	0.32	0.30	0.43	0.66	0.28
MgO	0.28	0.23	0.10	0.16	0.09	0.26	0.17	0.15	0.20	0.35	0.25	0.26	0.05	0.09	0.13	0.12
CaO	31.87	31.55	32.60	33.16	33.76	32.75	32.38	32.48	32.32	32.45	32.44	31.92	32.13	32.18	31.92	32.72
Na ₂ O	0.19	0.44	0.09	0.02	0.12	0.13	0.22	0.01	0.19	0.11	0.02	0.07	0.16	0.05	0.10	0.21
K ₂ O	0	0.08	0	0	0	0	0	0	0	0	0	0	0.03	0	0.06	0
Total	98.07	98.43	98.36	98.74	98.79	98.66	98.41	98.15	98.21	98.59	98.84	98.69	98.56	98.86	98.05	99.20
Number of cations on the basis of 12 O																
Si	2.97	2.98	2.96	2.96	2.92	2.97	2.97	2.96	2.97	2.99	2.94	2.96	2.95	2.98	2.94	2.97
Ti	0	0.01	0	0	0.01	0	0	0	0.01	0	0	0	0.01	0	0	0
Al	0.08	0.06	0.16	0.05	0.41	0.19	0.30	0.17	0.10	0.10	0.40	0	0.08	0.02	0.01	0
Fe ³⁺	1.94	1.94	1.87	1.98	1.64	1.83	1.71	1.85	1.92	1.90	1.63	2.02	1.94	1.99	2.03	2.02
Fe ²⁺	0.11	0.14	0.11	0.06	0.08	0.06	0.12	0.12	0.09	0.06	0.15	0.12	0.13	0.11	0.11	0.08
Mn	0.02	0.01	0.01	0.01	0	0.03	0.01	0	0.02	0.02	0.02	0.02	0.02	0.03	0.05	0.02
Mg	0.04	0.03	0.01	0.02	0.01	0.03	0.02	0.02	0.02	0.04	0.03	0.03	0.01	0.01	0.02	0.01
Ca	2.86	2.84	2.91	2.96	2.98	2.91	2.87	2.90	2.90	2.89	2.86	2.86	2.88	2.87	2.89	2.92
And	96.02	96.32	92.33	97.58	80.14	90.47	84.84	91.53	95.06	94.61	79.82	99.67	95.90	98.88	99.61	99.69
Gro	1.53	3.07	3.57	0.41	16.81	5.52	9.99	3.94	0.65	0.99	13.39	5.72	1.31	4.09	5.17	3.70
Pyr	1.16	0.95	0.41	0.65	0.36	1.06	0.69	0.61	0.82	1.44	1.00	1.07	0.21	0.37	0.54	0.49

Table 3. Electron microprobe analyses of garnet from the Hongshan deposit (wt %).

Sample	Garnet–Diopside Skarn									Diopside–Garnet Skarn								
	KT2-4296-10									KT3-4033-6								
	Core			→			Rim			Core			→			Rim		
SiO ₂	35.91	35.34	35.84	35.36	35.74	35.10	36.17	35.24	35.50	35.31	35.15	35.33	35.93	35.98	35.49	35.99	35.10	35.37
TiO ₂	1.32	0	0	0.17	0.06	0.11	0	0	0.01	0.09	0.05	0	0	0.10	0.01	0	0.05	0.12
Al ₂ O ₃	7.58	0.11	5.03	0.23	5.79	0	4.10	0.05	0.72	0.22	0.32	0.16	0.52	1.46	0	0.92	0.27	0.59
Cr ₂ O ₃	0	0.07	0	0	0	0.13	0.05	0	0.14	0.14	0.09	0	0	0.12	0	0	0.07	
FeO	19.83	29.49	24.02	30.12	22.04	29.71	24.81	30.17	29.45	30.10	29.93	29.94	29.80	28.06	29.65	29.64	30.16	28.94
MnO	0.56	0.37	0.36	0.20	0.35	0.24	0.33	0.36	0.49	0.33	0.36	0.22	0.17	0.23	0.55	0.31	0.47	0.43
MgO	0.13	0.07	0	0.07	0.00	0.13	0.12	0.07	0.06	0.24	0.30	0.23	0.16	0.27	0.30	0.16	0.33	0.18
CaO	33.45	32.42	32.75	32.66	32.00	33.15	33.04	32.19	32.13	31.95	32.15	32.09	32.38	32.39	31.83	31.49	31.97	32.48
Na ₂ O	0	0.18	0.05	0.08	0.09	0.12	0.04	0.14	0.12	0.07	0.16	0.07	0.01	0.11	0.18	0.08	0	0.19
K ₂ O	0	0	0	0	0	0	0	0	0.01	0.01	0	0.02	0	0	0	0	0	0
Total	98.78	98.05	98.05	98.89	96.07	98.69	98.66	98.22	98.63	98.46	98.51	98.06	98.97	98.72	98.01	98.59	98.42	98.30
Number of cation on the basis of 12 O																		
Si	2.91	2.97	2.96	2.95	2.99	2.94	2.97	2.96	2.97	2.96	2.95	2.97	2.98	2.98	2.98	3.00	2.94	2.96
Ti	0.08	0	0	0.01	0	0.01	0	0	0	0.01	0	0	0	0.01	0	0	0	0.01
Al	0.72	0.01	0.49	0.02	0.57	0	0.40	0	0.07	0.02	0.03	0.02	0.05	0.14	0.00	0.09	0.03	0.06
Fe ³⁺	1.29	2.00	1.54	2.00	1.43	2.03	1.62	2.02	1.94	1.99	2.00	2.01	1.96	1.86	2.01	1.91	2.01	1.96
Fe ²⁺	0.06	0.07	0.12	0.10	0.11	0.05	0.08	0.10	0.12	0.12	0.10	0.10	0.11	0.09	0.07	0.15	0.11	0.06
Mn	0.04	0.03	0.03	0.01	0.02	0.02	0.02	0.03	0.03	0.02	0.03	0.02	0.01	0.02	0.04	0.02	0.03	0.03
Mg	0.02	0.01	0	0.01	0	0.02	0.01	0.01	0.01	0.03	0.04	0.03	0.02	0.03	0.04	0.02	0.04	0.02
Ca	2.90	2.92	2.90	2.92	2.87	2.97	2.91	2.90	2.88	2.87	2.89	2.89	2.88	2.88	2.87	2.81	2.87	2.91
And	63.99	99.23	75.87	98.88	71.49	99.58	80.19	99.76	96.04	98.47	98.15	99.22	97.47	92.51	99.85	95.49	98.46	97.12
Gro	32.31	2.97	19.37	2.85	24.01	2.74	15.62	4.25	1.69	4.49	3.83	3.93	2.07	2.57	4.97	1.95	4.70	0.98
Pyr	0.52	0.29	0	0.29	0	0.53	0.48	0.29	0.25	0.99	1.23	0.95	0.66	1.11	1.25	0.66	1.35	0.74

Table 4. Electron microprobe analyses of diopside from the Hongshan deposit (wt %).

Sample	Garnet–Diopside Skarn			Garnet–Diopside Skarn			Diopside Skarn			Diopside Skarn		
	KT12-4170-13			KT4-4078-1			KT3-4033-6			KT2-4235-10		
SiO ₂	45.76	54.94	53.91	56.01	54.86	55.06	54.32	54.23	53.76	51.74	52.17	51.88
TiO ₂	0.01	0.01	0.01	0.01	0.01	0.01	0.01	0.01	0	0.01	0	0
Al ₂ O ₃	19.63	0.12	0.21	0.21	0.34	0.11	0.37	0.18	0.34	0.15	0.12	0.26
FeO	12.65	2.95	4.05	2.81	2.96	5.06	5.78	8.94	10.12	12.15	16.37	16.32
Cr ₂ O ₃	0.03	0.02	0.01	0.03	0.05	0.04	0.02	0.01	0.06	0.01	0.02	0.05
MnO	0.06	0.21	0.82	0.15	0.15	0.43	0.52	0.42	0.11	0.56	0.17	0.63
MgO	0.05	16.72	15.91	15.72	15.34	14.37	15.62	11.53	10.64	9.99	4.99	6.89
CaO	20.61	24.32	23.97	24.21	25.37	24.83	22.30	24.18	23.91	23.94	25.01	22.93
Na ₂ O	0.01	0.00	0.02	0.02	0.01	0.01	0.00	0.01	0.04	0.00	0.03	0.05
K ₂ O	0.01	0.01	0.00	0.01	0.02	0.01	0.02	0.01	0.01	0.01	0.03	0.02
Total	98.82	99.30	98.91	99.18	99.11	99.93	98.96	99.52	98.99	98.56	98.91	99.03
Number of cations on the basis of 6 O												
Si	1.73	2.01	2.00	2.05	2.02	2.03	2.01	2.04	2.04	2.00	2.05	2.03
Al(IV)	0.27	0	0	0	0	0	0	0	0	0	0	0
Al(VI)	0.60	0.01	0.01	0.01	0.01	0	0.02	0.01	0.02	0.01	0.01	0.01
Ti	0	0	0	0	0	0	0	0	0	0	0	0
Cr	0	0	0	0	0	0	0	0	0	0	0	0
Fe ³⁺	0	0	0	0	0	0	0	0	0	0	0	0
Fe ²⁺	0.42	0.09	0.13	0.09	0.09	0.16	0.18	0.28	0.32	0.39	0.54	0.54
Mn	0	0.01	0.03	0	0	0.01	0.02	0.01	0	0.02	0.01	0.02
Mg	0	0.91	0.88	0.86	0.84	0.79	0.86	0.65	0.60	0.58	0.29	0.40
Ca	0.83	0.95	0.95	0.95	1.00	0.98	0.89	0.97	0.97	0.99	1.05	0.96
Na	0	0	0	0	0	0	0	0	0	0	0	0
K	0	0	0	0	0	0	0	0	0	0	0	0
Di	0.67	90.37	85.31	90.34	89.73	82.24	81.45	68.49	64.70	58.30	34.68	41.80
Hd	98.88	8.98	12.20	9.17	9.78	16.36	17.00	30.10	34.92	39.85	64.65	56.02
Jo	0.46	0.65	2.50	0.49	0.50	1.40	1.54	1.42	0.38	1.86	0.67	2.17

Table 5. Electron microprobe analyses of actinolite from the Hongshan deposit (wt %).

Samples	SiO ₂	TiO ₂	Al ₂ O ₃	FeO	Cr ₂ O ₃	MnO	MgO	CaO	Na ₂ O	K ₂ O	Total
Diopside–actinolite skarn KT12-4170-19	55.08	0.02	1.11	8.03	0.13	0.11	20.08	12.53	0.30	0.04	97.43
	54.43	0.22	1.46	7.98	0.12	0.15	19.86	12.90	0.30	0	97.42
	54.76	0	1.32	7.07	0	0.09	20.32	12.88	0.33	0	96.77
Actinolite skarn KT2-4296-11	55.03	0.46	2.12	4.72	0.06	0.13	21.48	12.92	0.45	0.01	97.38
	56.23	0.03	0.93	4.95	0.09	0.13	21.95	13.09	0.25	0.02	97.67
	53.91	0.17	0.55	10.89	0.13	0.30	18.44	12.16	0.35	0.12	97.02
Cations on the basis of 23 oxygens	Si	Ti	Al	Fe ³⁺	Fe ²⁺	Cr ³⁺	Mn	Mg	Ca	Na	K
KT12-4170-19	7.71	0	0.18	0.41	0.53	0.01	0.01	4.19	1.88	0.08	0.01
	7.64	0.02	0.24	0.40	0.54	0.01	0.02	4.16	1.94	0.08	0
	7.70	0	0.22	0.35	0.49	0	0.01	4.26	1.94	0.09	0
KT2-4296-11	7.63	0.02	0.35	0.25	0.30	0.01	0.02	4.44	1.92	0.12	0
	7.76	0	0.15	0.31	0.27	0.01	0.02	4.52	1.94	0.07	0
	7.69	0.02	0.09	0.52	0.78	0.02	0.04	3.92	1.86	0.10	0.02

Table 6. Sm–Nd concentrations and isotopic ratios of the garnet from the Hongshan deposit.

Sample	Sm (µg/g)	Nd (µg/g)	147Sm/144Nd	143Nd/144Nd	Standard Error	εNd (t)
KT3-4033-7	5.760	44.50	0.0784	0.512127	0.000006	−8.78
WY-4296-1	0.192	1.12	0.1040	0.512128	0.000006	−8.81
KT2-4296-6	1.780	9.73	0.1105	0.512194	0.000006	−6.64
7ZK16-1	0.480	2.82	0.1030	0.512138	0.000006	−9.02
D40-6	12.900	49.10	0.1592	0.512155	0.000006	−8.84
D40-8	12.500	33.00	0.2300	0.512202	0.000006	−9.05
D21-5	0.873	5.22	0.1012	0.512073	0.000006	−0.97
D48-13	3.060	6.99	0.2648	0.512178	0.000006	−8.52
KT2-4235-10	0.503	2.39	0.1269	0.512135	0.000007	−9.11
KT2-4170-21	1.890	12.40	0.0922	0.512120	0.000007	−9.04

6. Discussion

6.1. Mineralogy and Geochemistry of Skarn Minerals

The identification and classification of the skarn deposits were based on their mineralogy [26]. The Hongshan deposit is featured with layered or stratabound Cu ores with their occurrence in accordance with the host volcano-sedimentary wall rocks of the Qugasi Formation, which has led to the conception of sedimentary or SEDEX origin for these ores [10,11]. However, the pervasively distributed skarn minerals, e.g., andraditic garnet (Figure 4a), diopside–hedenbergite pyroxene (Figure 4a), actinolite, in the layered Cu ores are similar to the typical skarn Cu deposits as a result of interaction between felsic intrusion and surrounding carbonate rocks [26]. The lithologic or bedding contacts may provide highly permeable and/or reactive layers for the infiltration and lateral movement of the skarn-forming fluids [27]. Other evidences including the vertical zonation of skarn minerals, from top to bottom, are biotite hornfels–pyroxene hornfels, marble, wollastonite skarn (Wo > Pyx–Grt), pyroxene skarn (Pyx > Grt), garnet skarn (Grt > Pyx), pyroxene skarn, pyroxene hornfels, and biotite hornfels [6].

The chemical composition of the skarn minerals can also be used to evaluate the oxidation state of the mineralization fluids [27]. Many skarn Cu deposits contain a high abundance of chalcopyrite, bornite, pyrite, and magnetite ± hematite, which are believed to have formed from a high oxygen fugacity environment [26]. However, the large proportions of pyrrhotite (>60% sulfide) in the Hongshan deposit tends to be much more reduced than other skarn Cu deposits [28]. The highly andraditic composition of garnet (Adr₁₀₀ to Adr₆₄Gr₃₂, Figure 4a) and diopsidic composition of pyroxene (Di₉₀Hd₉ to Di₁Hd₉₉, Figure 4b) indicate the prograde skarn minerals are formed under oxidized conditions as other skarn Cu deposits [26]. This suggest that the initial fluids during the

prograde stage are inherently oxidized as other skarn Cu deposits and the rapid descent of the fugacity in the retrograde stage could be led by other effective factors.

6.2. Timing of Mineralization

The layered skarn Cu ores and vein-type Mo–Cu ores are two dominant ores in the Hongshan deposit. The age of the vein-type Mo–Cu ores have been precisely constrained by molybdenite Re–Os ages, ranging from 77 to 81 Ma [9,11,12]. However, the age of the layered skarn Cu ores is still in dispute. The existence of Triassic intrusions in the deposit area led some authors to argue the main layered skarn ores were formed in the Triassic [29], similar with the Pulang and Xuejiping porphyry Cu deposits in the Zhongdian area [4]. Re–Os dating with pyrrhotite, however, yielded a Late Cretaceous age with large error 79 ± 16 Ma [9]. Considering the low closure temperature of Re–Os systems in the pyrrhotite (as low as 400 °C) [30], a more robust and convincing method should be considered.

Garnet crystals grow between 400 °C and ~700 °C [31] and the primary growth ages can survive from wide range of P–T metamorphism, such as amphibolite metamorphism [15,16]. The strong preference of the garnet lattice for Sm over Nd makes Sm–Nd dating in garnet as a highly suitable chronometer for more than 30 years [16]. The garnets in the Hongshan deposit showed consistent or typical oscillatory zonations (Figure 5), indicating they were formed from a single hydrothermal system that underwent chemical fluctuation. The low $^{147}\text{Sm}/^{144}\text{Nd}$ ratios of 0.07 to 0.26 for the garnet samples (Table 6) in the Hongshan deposit indicated some silicate inclusions, such as epidote and pyroxene, might not be completely removed when compared with the inclusion-free garnet with high $^{147}\text{Sm}/^{144}\text{Nd}$ ratios (>1) [16,32]. Since these inclusions grew in isotopic equilibrium with the surrounding garnet and rock matrix during prograde metamorphism, the requirements of isochron dating are fulfilled. Therefore, the well-constrained isochron age of 76.48 ± 7.29 Ma (MSWD = 1.2) (Figure 6b) revealed from seven garnet separates can represent the crystallization time of the garnet. This age was consistent with the Re–Os age for the pyrrhotite from the layered skarn ores, and thereby indicated that the layered skarn mineralization was formed in the Late Cretaceous, rather than in the Triassic as previously thought [9]. The coincidence of the geochronology from the layered skarn ores and vein-type mineralization further indicated that both ores were the result of a single genetic event, rather than multiple events [10,11]. The development of endoskarn in the quartz monzonite porphyry (Figure 3a) and granite porphyry indicated the Cu–Mo mineralization in the Hongshan deposit was plausibly related to the syntectonic intrusions.

6.3. Implication for the Regional Metallogeny

The metallogenic age of the Hongshan deposit is constrained from the Sm–Nd dating of garnet and previous data to be Late Cretaceous. The Hongshan skarn Cu–Mo deposit, associated with the Xiuwacu quartz vein W–Mo, Relin quartz vein W–Mo, and Tongchanggou porphyry Mo–Cu deposit [8,33–35], thus defined a roughly N–S trending Late Cretaceous porphyry belts in the Zhongdian area, locally overlapping the Late Triassic porphyry belt (Figure 1c). Numerous geochemical research on the related intrusions revealed that the Zhongdian area in the Late Cretaceous underwent post-collisional extension event, which was also recently recognized as an optimal setting for the formation of porphyry–skarn deposits [36–38]. During post-collisional extension setting, remobilization of chalcophile metals from metasomatized mantle lithosphere have led to the generation of fertile magmas capable of forming porphyry–skarn Cu–Mo–W deposits in the Zhongdian area [17,33].

7. Conclusions

Two types of Cu–Mo ores, mainly developed in the skarns, have been recognized in the Hongshan deposit, i.e., massive or layered skarn (Figure 3a) and vein-type, with the former being dominant. The highly andraditic composition of garnet (Adr_{100} to $\text{Adr}_{64}\text{Gr}_{32}$) and diopsidic composition of pyroxene ($\text{Di}_{90}\text{Hd}_9$ to $\text{Di}_1\text{Hd}_{99}$) indicate the layered skarn ores are magmatic-hydrothermal origin that formed under oxidized conditions. Sm–Nd dating of garnet yielded an isochron age of 76.48 ± 7.29 Ma

for the layered skarn ores, indicating the Hongshan deposit was formed in the Late Cretaceous in a unified system rather than from multiple mineralization events. The recognition of the Late Cretaceous post-collisional porphyry–skarn Cu–Mo–W belt in the Zhongdian area exhibits a promising prospecting potential.

Author Contributions: Data curation, B.Z. and Y.Z.; funding acquisition, B.Z. and C.X.; project administration, B.Z.; software, C.D.; supervision, C.X.; writing—original draft, B.Z.

Funding: This work was supported by National Key Research and Development Program of China (2017YFC0601202), National Science Foundation of China (41802108), and Fundamental Research Funds for the Central Universities (CUGL170812).

Acknowledgments: We would like to thank Sinacili, Baimakangzhu, He Jianwen, and Lurongcili from the Hongshan deposit for the help in the field. The editor and two reviewers are thanked for their constructive and detailed review of this manuscript.

Conflicts of Interest: The authors declare no conflict of interest.

References

- Deng, J.; Wang, Q.; Li, G.; Santosh, M. Cenozoic tectono-magmatic and metallogenic processes in the Sanjiang region, southwestern China. *Earth-Sci. Rev.* **2014**, *138*, 268–299. [[CrossRef](#)]
- Hou, Z.; Zaw, K.; Pan, G.; Mo, X.; Xu, Q.; Hu, Y.; Li, X. Sanjiang Tethyan metallogenesis in S.W. China: Tectonic setting, metallogenic epochs and deposit types. *Ore Geol. Rev.* **2007**, *31*, 48–87. [[CrossRef](#)]
- Mao, J.; Pirajno, F.; Lehmann, B.; Luo, M.; Berzina, A. Distribution of porphyry deposits in the Eurasian continent and their corresponding tectonic settings. *J. Asian Earth Sci.* **2014**, *79*, 576–584. [[CrossRef](#)]
- Li, W.; Zeng, P.; Hou, Z.; White, N.C. The Pulang porphyry copper deposit and associated felsic intrusions in Yunnan Province, Southwest China. *Econ. Geol.* **2011**, *106*, 79–92.
- Leng, C.; Cooke, D.R.; Hou, Z.; Evans, N.J.; Zhang, X.; Chen, W.T.; Danišik, M.; McInnes, B.I.A.; Yang, J. Quantifying Exhumation at the Giant Pulang Porphyry Cu–Au Deposit Using U–Pb–He Dating. *Econ. Geol.* **2018**, *113*, 1077–1092. [[CrossRef](#)]
- Peng, H.; Mao, J.; Hou, L.; Shu, Q.; Zhang, C.; Liu, H.; Zhou, Y. Stable Isotope and Fluid Inclusion Constraints on the Source and Evolution of Ore Fluids in the Hongniu-Hongshan Cu Skarn Deposit, Yunnan Province, China. *Econ. Geol.* **2016**, *111*, 1369–1396. [[CrossRef](#)]
- Wang, X.; Hu, R.; Bi, X.; Leng, C.; Pan, L.; Zhu, J.; Chen, Y. Petrogenesis of Late Cretaceous I-type granites in the southern Yidun Terrane: New constraints on the Late Mesozoic tectonic evolution of the eastern Tibetan Plateau. *Lithos* **2014**, *208*, 202–219. [[CrossRef](#)]
- Yang, L.; Deng, J.; Gao, X.; He, W.; Meng, J.; Santosh, M.; Yu, H.; Yang, Z.; Wang, D. Timing of formation and origin of the Tongchanggou porphyry–skarn deposit: Implications for Late Cretaceous Mo–Cu metallogenesis in the southern Yidun Terrane, SE Tibetan Plateau. *Ore Geol. Rev.* **2016**, *81*, 1015–1032. [[CrossRef](#)]
- Zu, B.; Xue, C.; Zhao, Y.; Qu, W.; Li, C.; Symons, D.T.A.; Du, A. Late Cretaceous metallogeny in the Zhongdian area: Constraints from Re–Os dating of molybdenite and pyrrhotite from the Hongshan Cu deposit, Yunnan, China. *Ore Geol. Rev.* **2015**, *64*, 1–12. [[CrossRef](#)]
- Leng, C. Genesis of Hongshan Cu polymetallic large deposit in the Zhongdian area, NW Yunnan: Constraints from LA-ICP-MS trace elements of pyrite and pyrrhotite. *Earth Sci. Front.* **2017**, *24*, 162–175.
- Xu, X.; Cai, X.; Qu, W.; Song, B.; Qin, K.; Zhang, B. Later Cretaceous granitic porphyritic Cu–Mo mineralization system in the Hongshan area, northwestern Yunnan and its significances for tectonics. *Acta Geol. Sin.* **2006**, *80*, 1422–1433.
- Peng, H.; Mao, J.; Pei, R.; Zhang, C.; Tian, G.; Zhou, Y.; Li, J.; Hou, L. Geochronology of the Hongniu-Hongshan porphyry and skarn Cu deposit, northwestern Yunnan province, China: Implications for mineralization of the Zhongdian arc. *J. Asian Earth Sci.* **2014**, *79*, 682–695. [[CrossRef](#)]
- Stein, H.J.; Morgan, J.W.; Scherstén, A. Re–Os dating of low-level highly radiogenic (LLHR) sulfides: The Harnäs gold deposit, southwest Sweden, records continental-scale tectonic events. *Econ. Geol.* **2000**, *95*, 1657–1671. [[CrossRef](#)]
- Li, Y.; Li, J.; Li, X.; Selby, D.; Huang, G.; Chen, L.; Zheng, K. An Early Cretaceous carbonate replacement origin for the Xinqiao stratabound massive sulfide deposit, Middle-Lower Yangtze Metallogenic Belt, China. *Ore Geol. Rev.* **2017**, *80*, 985–1003. [[CrossRef](#)]

15. Baxter, E.F.; Scherer, E.E. Garnet Geochronology: Timekeeper of Tectonometamorphic Processes. *Elements* **2013**, *9*, 433–438. [[CrossRef](#)]
16. Baxter, E.F. Garnet: A Rock-Forming Mineral Petrochronometer. *Rev. Miner. Geochem.* **2017**, *83*, 469–553. [[CrossRef](#)]
17. Zu, B.; Xue, C.; Chi, G.; Zhao, X.; Li, C.; Zhao, Y.; Yalikun, Y.; Zhang, G.; Zhao, Y. Geology, geochronology and geochemistry of granitic intrusions and the related ores at the Hongshan Cu-polymetallic deposit: Insights into the Late Cretaceous post-collisional porphyry-related mineralization systems in the southern Yidun arc, SW China. *Ore Geol. Rev.* **2016**, *77*, 25–42. [[CrossRef](#)]
18. Li, W.; Yu, H.; Gao, X.; Liu, X.; Wang, J. Review of Mesozoic multiple magmatism and porphyry Cu–Mo (W) mineralization in the Yidun Arc, eastern Tibet Plateau. *Ore Geol. Rev.* **2017**, *90*, 795–812. [[CrossRef](#)]
19. Hou, Z.; Yang, Y.; Qu, X.; Huang, D.; Lv, Q.; Wang, H.; Yu, J.; Tang, S. Tectonic evolution and mineralization systems of the Yidun arc orogen in Sanjiang region. *Acta Geol. Sin.* **2004**, *78*, 109–120.
20. Yang, L.; He, W.; Gao, X.; Xie, S.; Yang, Z. Mesozoic multiple magmatism and porphyry–skarn Cu–polymetallic systems of the Yidun Terrane, Eastern Tethys: Implications for subduction- and transtension-related metallogeny. *Gondwana Res.* **2018**, *62*, 144–162. [[CrossRef](#)]
21. Chen, J.; Xu, J.; Ren, J.; Huang, X.; Wang, B. Geochronology and geochemical characteristics of Late Triassic porphyritic rocks from the Zhongdian arc, eastern Tibet, and their tectonic and metallogenic implications. *Gondwana Res.* **2014**, *26*, 492–504. [[CrossRef](#)]
22. Gao, X.; Yang, L.; Orovan, E.A. The lithospheric architecture of two subterrane in the eastern Yidun Terrane, East Tethys: Insights from Hf–Nd isotopic mapping. *Gondwana Res.* **2018**, *62*, 127–143. [[CrossRef](#)]
23. Wang, X.; Bi, X.; Leng, C.; Zhong, H.; Tang, H.; Chen, Y.; Yin, G.; Huang, D.; Zhou, M. Geochronology and geochemistry of Late Cretaceous igneous intrusions and Mo–Cu–(W) mineralization in the southern Yidun Arc, SW China: Implications for metallogenesis and geodynamic setting. *Ore Geol. Rev.* **2014**, *61*, 73–95. [[CrossRef](#)]
24. Peng, H.; Zhang, C.; Mao, J.; Santosh, M.; Zhou, Y.; Hou, L. Garnets in porphyry–skarn systems: A LA–ICP–MS, fluid inclusion, and stable isotope study of garnets from the Hongniu–Hongshan copper deposit, Zhongdian area, NW Yunnan Province, China. *J. Asian Earth Sci.* **2015**, *103*, 229–251. [[CrossRef](#)]
25. Vermeesch, P. IsoplotR: A free and open toolbox for geochronology. *Geosci. Front.* **2018**, *9*, 1479–1493. [[CrossRef](#)]
26. Meinert, L.D.; Dipple, G.M.; Nicolescu, S. World Skarn Deposits. *Econ. Geol.* **2005**, *100*, 299–336.
27. Maher, K.C. Skarn alteration and mineralization at corocohuayco, Tintaya District, Peru. *Econ. Geol.* **2010**, *105*, 263–283. [[CrossRef](#)]
28. Zu, B.; Xue, C.; Yaxiaer, Y.; Wang, Q.; Liang, H.; Zhao, Y.; Liu, M. Sulfide zonal texture and its geological significance of ores from the Hongshan copper deposit in Shangri-la, Yunnan Province, China. *Acta Petrol. Sin.* **2013**, *29*, 1203–1213.
29. Wang, S.; Zhang, X.; Leng, C.; Qin, C.; Wang, W.; Zhao, M. Stable isotopic compositions of the Hongshan skarn copper deposit in the Zhongdian area and its implication for the copper mineralization process. *Acta Petrol. Sin.* **2008**, *24*, 480–488.
30. Brenan, J.M.; Cherniak, D.J.; Rose, L.A. Diffusion of osmium in pyrrhotite and pyrite: Implications for closure of the Re–Os isotopic system. *Earth Planet. Sci. Lett.* **2000**, *180*, 399–413. [[CrossRef](#)]
31. Caddick, M.J.; Kohn, M.J. Garnet: Witness to the Evolution of Destructive Plate Boundaries. *Elements* **2013**, *9*, 427–432. [[CrossRef](#)]
32. Mühlberg, M.; Hegner, E.; Klemm, R.; Pfänder, J.A.; Kaliwoda, M.; Biske, Y.S. Late Carboniferous high-pressure metamorphism of the Kassan Metamorphic Complex (Kyrgyz Tianshan) and assembly of the SW Central Asian Orogenic Belt. *Lithos* **2016**, *264*, 41–55.
33. Yang, L.; Gao, X.; Shu, Q. Multiple Mesozoic porphyry–skarn Cu (Mo–W) systems in Yidun Terrane, east Tethys: Constraints from zircon U–Pb and molybdenite Re–Os geochronology. *Ore Geol. Rev.* **2017**, *90*, 813–826. [[CrossRef](#)]
34. Gao, X.; Yang, L.; Meng, J.; Zhang, L. Zircon U–Pb, molybdenite Re–Os geochronology and Sr–Nd–Pb–Hf–O–S isotopic constraints on the genesis of Relin Cu–Mo deposit in Zhongdian, Northwest Yunnan, China. *Ore Geol. Rev.* **2017**, *91*, 945–962. [[CrossRef](#)]

35. He, J.; Wang, B.; Wang, L.; Wang, Q.; Yan, G. Geochemistry and geochronology of the Late Cretaceous Tongchanggou Mo–Cu deposit, Yidun Terrane, SE Tibet; implications for post-collisional metallogenesis. *J. Asian Earth Sci.* **2018**, *172*, 308–327. [[CrossRef](#)]
36. Hou, Z.; Zhang, H.; Pan, X.; Yang, Z. Porphyry Cu (–Mo–Au) deposits related to melting of thickened mafic lower crust: Examples from the eastern Tethyan metallogenic domain. *Ore Geol. Rev.* **2011**, *39*, 21–45. [[CrossRef](#)]
37. Richards, J.P. Postsubduction porphyry Cu–Au and epithermal Au deposits: Products of remelting of subduction-modified lithosphere. *Geology* **2009**, *37*, 247–250. [[CrossRef](#)]
38. Richards, J.P. Magmatic to hydrothermal metal fluxes in convergent and collided margins. *Ore Geol. Rev.* **2011**, *40*, 1–26. [[CrossRef](#)]



© 2019 by the authors. Licensee MDPI, Basel, Switzerland. This article is an open access article distributed under the terms and conditions of the Creative Commons Attribution (CC BY) license (<http://creativecommons.org/licenses/by/4.0/>).